INSTITUTE OF PHYSICS PUBLISHING JOURNAL OF PHYSICS B: ATOMIC, MOLECULAR AND OPTICAL PHYSICS

J. Phys. B: At. Mol. Opt. Phys. **39** (2006) 2917–2937 doi:10.1088/0953-4075/39/14/001

Large-scale calculation of dielectronic recombination parameters for Mg-like Fe

I Murakami[1], T Kato[1], D Kato[1], U I Safronova[2], T E Cowan[2] and Yu Ralchenko[3]

[1] National Institute for Fusion Science, Toki, Gifu 509-5292, Japan
[2] Physics Department, University of Nevada, Reno, NV 89557, USA
[3] National Institute of Standards and Technology, Gaithersburg, MD 20899-8422, USA

E-mail: usafrono@nd.edu

Received 3 April 2006
Published 30 June 2006
Online at stacks.iop.org/JPhysB/39/2917

Abstract

Energy levels, radiative transition probabilities and autoionization rates for $1s^2 2s^2 2p^6 3l'nl$ ($n = 3$–12, $l \leqslant n-1$) and $1s^2 2s^2 2p^6 4l'nl$ ($n = 4$–7, $l \leqslant n-1$) states in Mg-like iron (Fe^{14+}) are calculated by the Hartree–Fock-relativistic method (Cowan code) and the relativistic many-body perturbation theory method (RMBPT code). Autoionizing levels above three thresholds $1s^2 2s^2 2p^6 3s$, $1s^2 2s^2 2p^6 3p$ and $1s^2 2s^2 2p^6 3d$ are considered. It is found that configuration mixings [3sns + 3pnp + 3dnd] and [3snp + 3pns + 3pnd + 3dnp] play an important role for all atomic characteristics. Branching ratios relative to the first threshold and intensity factors are calculated for satellite lines, and dielectronic recombination (DR) rate coefficients are determined for the excited 444 odd-parity and 419 even-parity states. It is shown that the contribution of the highly-excited states is very important for calculation of total DR rates. Contributions from the excited $1s^2 2s^2 2p^6 3l'nl$ states with $n \geqslant 12$ and $1s^2 2s^2 2p^6 4l'nl$ states with $n \geqslant 7$ to DR rate coefficients are estimated by extrapolation of all atomic parameters. The total DR rate coefficient is derived as a function of electron temperature.

(Some figures in this article are in colour only in the electronic version)

1. Introduction

Dielectronic satellites (DS) are spectral lines that correspond to the same transitions as the resonance lines, but occur in the presence of additional electrons. For instance, satellites to resonance lines of Ne-like ions could be created by transitions from doubly-excited states of Na-like and other lower-charge ions. DS often serve as an important tool for plasma diagnostics and as a test bed for atomic structure theories. An example of DS can be provided

by the DS lines from Fe XVI (Na-like) and Fe XV (Mg-like) in the vicinity of the strong 2p–3d transitions of Fe XVII (Ne-like) that were recently recorded from plasmas created in three different laser facilities [1].

There are numerous theoretical and experimental studies devoted to dielectronic satellites and dielectronic recombination of Na-like ions. For instance, the DR rate coefficients were calculated for Ar, Fe and Mo target ions of the Na isoelectronic sequence [2] with both $\Delta n = 0$ and $\Delta n = 1$ transitions included and assuming pure LS coupling. The DR rate coefficients of the Fe^{15+} ion were also studied in the isolated-resonance, distorted-wave approximation in [3]. The cross-section calculations included dielectronic transitions associated with the 3s–3l and 3s–4l excitations. The energy-averaged $\Delta n = 1$ cross sections were also presented in [3] as a function of electron energy. The effect of the configuration interaction (CI) between resonances for the dielectronic recombination and resonant transfer excitation of Na-like ions was investigated in [4], where CI between the $1s^22s^22p^53s3d4p$ and $1s^22s^22p^53p^24p$ configurations was included to analyse the $1s^22s^22p^53s3d4p$ resonances. As for the experimental efforts, the absolute rates and cross sections for dielectronic recombination and ionization of Na-like Fe^{15+} ($1s^22s^22p^63s$) ion were measured at electron impact energies between 0 and 1030 eV using the Heidelberg heavy ion storage ring TSR with the cooling device as an electron target [5]. The doubly-excited intermediate states ($1s^22s^22p^53snln'l'$) formed in the first step of the resonant-excitation-double-autoionization process decay alternatively by the emission of photons rather than electrons. The total process was considered as a dielectronic recombination process [5].

The effect of the low-temperature $\Delta n = 0$ dielectronic recombination on the relative populations of the Fe M-shell states was recently investigated in [6]. The ionization structure and temperature in cosmic plasmas depend strongly on ionization and recombination processes. Recombination can occur via radiative recombination, charge transfer, or dielectronic recombination. It was pointed out in [6] that the low-temperature DR rates are available for the first four ionization states of the C, N and O sequences, but there are no similar DR data for the M-shell ions of Fe. The iron unresolved transition arrays in active galactic nuclei were recently studied in [7] where simulations of photoionized plasmas failed to predict the level of ionization of iron. The discrepancy was attributed to underestimation of the low-temperature DR rates for iron M-shell ions. Also, DR rate coefficients for Na-like ions of elements with $12 \leqslant Z \leqslant 30$ were calculated in the independent-process isolated-resonance approximation [8]. Both $\Delta n = 0$ and $\Delta n > 0$ core excitation DR channels were taken into account in determination of the total DR rate coefficients.

In the present paper we report the state-selective DR rate coefficients to excited states of Mg-like iron as well as the total DR rate coefficients. While the DR channel due to excitation of $n = 2$ electrons is known to be of importance (see, e.g., [9–11]), here we restrict our calculations to the most important channel due to excitation of the outer 3s electron. The DR rate coefficients are calculated including $1s^22s^22p^63l'nl$ ($n = 3$–12, $l' \leqslant 2, l \leqslant n - 1$) and $1s^22s^22p^64l'nl$ ($n = 4$–7, $l' \leqslant 3, l \leqslant n - 1$) states. Contributions from the autoionizing $1s^22s^22p^63l'nl$ states with $n \geqslant 12$ and from the autoionizing $1s^22s^22p^64l'nl$ states with $n \geqslant 7$ are estimated by extrapolation of all atomic characteristics and used to derive the DR rate coefficients for excited states and the total DR rate coefficients as a function of electron temperature. (Below we omit the core $1s^22s^22p^6$ from the configuration notation.) The energy levels, transition probabilities and autoionization rates required for calculation of the DR parameters are determined as well. The present paper continues our efforts on the calculation of the low-temperature DR rate coefficients that were previously determined for C I [12], C II [13, 14], C III [15], O IV [16], O V [17] and Ne VII [18].

The customary energy units cm^{-1} and eV used in this paper are related to the SI units via $1\ cm^{-1} = 1.986\,445\,61(34) \times 10^{-23}$ J and $1\ eV = 1.602\,176\,53(14) \times 10^{-19}$ J [19].

2. Energy levels, transition probabilities and autoionization rates

Determination of dielectronic recombination rate coefficients necessarily includes calculation of atomic parameters for intermediate and final states. Therefore, we calculated the energies, radiative and autoionization rates for the intermediate states $3l'nl$ ($n = 3$–12, $l' \leqslant 2$, $l \leqslant n-1$) and $4l'nl$ ($n = 4$–7, $l' \leqslant 3$, $l \leqslant n-1$) states in Mg-like iron (Fe^{14+}). The complete list includes 222 $3lnl'$ configurations (total of 2285 levels) and 82 $4lnl'$ configurations. Due to computational issues, the calculation of the DR parameters involving $4lnl'$ states was performed with account of the $3lnl'$ states with $n \leqslant 8$ only. The resulting list of levels, included in the set of $3lnl'$ configurations with $n = 3$–12, consists of 929 even-parity and 976 odd-parity states, while the set of $4lnl'$ ($n = 4$–7) and $3lnl'$ ($n = 3$–8) configurations contains 905 even-parity and 979 odd-parity states.

The atomic energy levels, radiative transition probabilities and autoionization rates were calculated using the atomic structure code by Cowan [20, 21]. The scaling of electrostatic integrals in the Cowan code allows us to effectively account for correlation effects and obtain good agreement with experimental energies. We used one scaling factor (0.85) for all electrostatic integrals. In order to simplify calculations, radiative transitions with small probabilities $A_r \leqslant 10^5$ s^{-1} were removed from consideration. Even with this limitation the resulting list includes 172 692 radiative transitions between the $3ln_1l_1$ and $3l'n_2l_2$ (with $n_1, n_2 = 3$–12; $l_1 \leqslant n_1 - 1$, $l_2 \leqslant n_2 - 1$; $l, l' =$ s, p, d) states and 165 806 transitions between the $3ln_1l_1$ and $4l'n_2l_2$ (with $n_1 = 3$–12, $l_1 \leqslant n_1 - 1$, $n_2 = 4$–7; $l_2 \leqslant n_2 - 1$; $l =$ s, p, d; $l' =$ s, p, d, f) states.

To better evaluate the Cowan code results that were primarily used in determination of the DR rate coefficients, the energies and radiative transition probabilities were also calculated by the relativistic many-body perturbation theory method (RMBPT code). This method was described in detail in [22, 23].

The results of calculations are presented in tables 1–6. In tables 1 and 2, the theoretical (Cowan and RMBPT) energies for the $3l3l'$ and $3l4l'$ levels of Fe^{14+} ion are compared with the NIST recommended data [24] and other theoretical $3l3l'$ and $3l4l'$ excitation energies [25–27]. The other methods selected for comparisons include the general relativistic atomic structure package (GRASP code) [27], the configuration interaction with relativistic corrections method implemented in the CIV3 code [26, 27], and the SUPERSTRUCTURE code based on a scaled Thomas–Fermi potential approach [25]. Those data are given in columns 'GRASP', 'CIV3' and 'SPSTR' of tables 1 and 2.

As one can see from table 1, on the average, the smallest differences between the theoretical calculations and the NIST recommended data are for the present results obtained by the RMBPT code (about 0.1%). A slightly worse agreement of about 0.1%–0.3% is noticed for the CIV3 results. As for the specific levels, the largest disagreement between theoretical calculations and NIST data is for the $3s3d\ ^1D_2$ level: 1000 cm^{-1} for the RMBPT and CIV3 codes, 10 000 cm^{-1} for the Cowan and GRASP codes and 15 000 cm^{-1} for the SUPERSTRUCTURE code. On the other hand, the best agreement was found for the $3p^2\ ^1D_2$ level: 6 cm^{-1} for the RMBPT code, 612 cm^{-1} for the GRASP code and 752 cm^{-1} for the SUPERSTRUCTURE code.

The RMBPT and CIV3 [26, 27] results given in table 2 for the $3s4l'$ states agree better with the NIST recommended data [24] than the results obtained by the GRASP [27] and SUPERSTRUCTURE [25] codes. Unfortunately, there are only few available NIST energies for the 3p4f states and no data are available for the 3p4s, 3p4p and 3p4d states. It should be noted that there is a large disagreement of about 3000 cm^{-1}–15 000 cm^{-1} between the RMBPT and CIV3 results for the $3p4l'$ states. This difference could be attributed to the correlation

Table 1. Energies (10^3 cm^{-1}) for the $3l3l'$ excited states of Mg-like Fe. Comparison of theoretical results (Cowan and RMBPT codes) with the NIST recommended data [24] and theoretical results obtained by the CIV3 [27], GRASP [27] and SUPERSTRUCTURE [25] codes.

Level		E (10^3 cm^{-1})					
Configuration	*LSJ*	COWAN	RMBPT	CIV3	GRASP	SPSTR	NIST
$3s^2$	$^1S_0$	0.000	0.000	0.000	0.000	0.000	0.000
3s3p	$^3P_0$	233.897	233.839	234.692	232.915	231.809	233.910
3s3p	$^3P_1$	239.497	239.682	240.391	238.767	237.563	239.662
3s3p	$^3P_2$	253.079	253.853	254.589	252.805	251.167	253.820
3s3p	$^1P_1$	342.730	351.804	351.307	357.088	355.538	351.914
$3p^2$	$^3P_0$	555.683	554.498	555.447	556.986	558.887	554.500
$3p^2$	$^1D_2$	562.242	559.596	561.741	560.202	560.342	559.590
$3p^2$	$^3P_1$	565.490	564.565	565.415	566.818	567.956	564.570
$3p^2$	$^3P_2$	582.386	581.776	582.983	583.568	584.013	581.690
$3p^2$	$^1S_0$	651.744	659.446	662.902	666.323	683.314	660.970
3s3d	$^3D_1$	678.018	678.264	679.542	681.603	681.728	678.830
3s3d	$^3D_2$	679.245	679.293	680.466	682.597	682.981	679.785
3s3d	$^3D_3$	681.142	680.882	682.092	684.151	683.314	681.410
3s3d	$^1D_2$	752.851	761.190	761.165	772.607	777.871	762.163
3p3d	$^3F_2$	931.628	927.837	930.170	930.067	931.063	928.420
3p3d	$^3F_3$	941.180	937.708	938.996	939.836	940.584	938.180
3p3d	$^3F_4$	952.319	949.235	963.516	950.964	951.506	949.660

Table 2. Energies (10^3 cm^{-1}) for the $3l4l'$ excited states of Mg-like Fe. Comparison of theoretical results (Cowan and RMBPT codes) with recommended NIST data [24] and theoretical results obtained by the CIV3 [27], GRASP [27] and SUPERSTRUCTURE [25] codes.

Level			E (10^3 cm^{-1})				
Configuration	*LSJ*	COWAN	RMBPT	CIV3	GRASP	SPSTR	NIST
3s4s	$^3S_1$	1761.322	1764.503	1764.376	1761.477	1764.348	1763.700
3s4p	$^1P_1$	1888.048	1890.725	1890.775	1888.243	1891.923	1889.970
3s4d	$^3D_1$	2030.134	2032.654	2032.073	2030.386	2033.983	2031.310
3s4d	$^3D_2$	2030.817	2033.440	2032.768	2095.191	2034.767	2032.020
3s4d	$^3D_3$	2032.010	2034.691	2033.913	2032.355	2035.999	2033.180
3s4d	$^1D_2$	2033.416	2036.452	2036.031	2034.579	2038.294	2035.280
3s4f	$^3F_2$	2104.407	2108.884	2109.238	2107.314	2111.952	2108.520
3s4f	$^3F_3$	2104.618	2109.088	2109.320	2107.522	2112.194	2108.620
3s4f	$^3F_4$	2104.904	2109.377	2109.577	2107.817	2112.517	2108.880
3s4f	$^1F_3$	2118.274	2122.775	2123.925	2125.923	2130.264	2123.150
3p4f	$^3G_3$	2377.958	2380.511	2383.688	2380.143	2385.765	2380.160
3p4f	$^3G_4$	2384.270	2387.222	2402.178	2400.028	2392.747	2386.700
3p4f	$^3G_5$	2399.277	2402.678	2412.816	2386.343	2407.911	2402.100

corrections that were discussed with regard to the $3l3l'$ states in Mg-like ions in [23]. Note also that the second-order contribution calculated with the RMBPT code is quite large and reaches about 10 000 cm^{-1}–30 000 cm^{-1} for different states.

As can be seen from table 2, the difference in energy for the three 3p4f ^3G_J levels between the RMBPT and NIST data (350 cm^{-1}–580 cm^{-1}) is smaller than that between the CIV3 and

Table 3. Energies (10^3 cm^{-1}), sum of weighted radiative transition rates ($\sum gA_r$ in s^{-1}), and weighted autoionization rates (gA_a in s^{-1}) for the $4l4l'$ excited states of Mg-like Fe calculated by the Cowan (a) and RMBPT (b) codes. Notation x [y] in all tables means $x \times 10^y$.

Level		E (10^3 cm^{-1})			gA_a (s^{-1})	
				$\sum gA_r$ (s^{-1})	3s	3p
Configuration	*LSJ*	a	b	a	a	a
$4s^2$	$^1S_0$	3604.647	3606.320	6.137 [11]	0.000 [00]	0.000 [00]
4s4p	$^3P_0$	3691.536	3693.018	5.412 [11]	2.448 [13]	0.000 [00]
4s4p	$^3P_1$	3693.798	3695.390	1.626 [12]	7.435 [13]	0.000 [00]
4s4p	$^3P_2$	3699.079	3700.893	2.719 [12]	1.218 [14]	0.000 [00]
4s4p	$^1P_1$	3743.639	3750.241	1.684 [12]	2.678 [14]	0.000 [00]
$4p^2$	$^1D_2$	3817.442	3816.662	2.724 [12]	3.982 [13]	0.000 [00]
4s4d	$^1D_2$	3897.832	3900.939	3.228 [12]	3.440 [14]	0.000 [00]
4s4f	$^3F_2$	3925.285	3925.744	5.585 [12]	1.057 [14]	0.000 [00]
4s4f	$^3F_3$	3926.036	3926.764	7.927 [12]	1.488 [14]	0.000 [00]
4p4d	$^3P_0$	3981.568	3986.741	6.318 [11]	4.392 [12]	7.283 [13]
4p4f	$^1F_3$	4036.062	4039.419	8.305 [12]	3.918 [12]	7.290 [13]
$4d^2$	$^1S_0$	4158.605	4166.260	8.264 [11]	3.496 [13]	1.477 [14]
4d4f	$^1G_4$	4174.384	4176.092	1.176 [13]	1.146 [11]	5.641 [11]
$4f^2$	$^3H_4$	4255.961	4260.225	1.658 [13]	3.784 [11]	2.064 [14]

NIST data (3500 cm^{-1}–15 500 cm^{-1}) by a factor of 10–20. Note also that the difference between our RMBPT and COWAN data is about 2000 cm^{-1}–3000 cm^{-1} for all $3l4l'$ states.

In table 3, we compare our results for energies of the $4l4l'$ states obtained by the two codes, Cowan and RMBPT (columns (a) and (b), respectively). Unfortunately, there exist no recommended data for the $4l4l'$ states. One can see from table 3 that the agreement between the results obtained by the two codes is, on average, within several thousands of cm^{-1} with generally better results for triplet states (see, e.g., [22] for a discussion of correlation corrections for singlets and triplets in Be-like ions). In table 3, the weighted sum of radiative transition rates $\left(\sum gA_r \text{ in s}^{-1}\right)$, and the weighted autoionization rates (gA_a in s^{-1}) for the $4l4l'$ excited states of Mg-like Fe below the first 3s threshold ($I = 3686\,000$ cm^{-1}) and the second 3p threshold ($I = 3963\,000$ cm^{-1}) are also presented. It was found that the $4l4l'$ excited states in Fe^{14+} have energies smaller than the third 3d threshold ($I = 4361\,000$ cm^{-1}). Also, the 4s4p ^3P_J levels are located just above the first threshold (within 13 000 cm^{-1}) and the $4s^2$ $^1S_0$ state is not autoionizing at all.

In table 4, the wavelengths λ (in Å) and radiative transition rates A_r (in units of 10^8 s^{-1}) for the 3s3p–$3p^2$, 3s3p–3s3d and 3s3d–3p3d transitions are presented. Both LS-allowed (triplet–triplet and singlet–singlet) and intercombination (triplet–singlet) transitions are included here. Our results, obtained from the Cowan (columns 5 and 8) and RMBPT (columns 6 and 9) codes, can be compared with the NIST recommended data [24] shown in columns 7 and 10. The uncertainties in the recommended values were estimated to be less than 10% based on comparisons with experimental results from the lifetime and emission measurements. The present theoretical results are seen to agree with each other and with the NIST data at the 10%–30% level.

The Cowan code results as well as the NIST data for the $3s^2$–3s4p, 3s3p–3s4d, 3s3p–3s4s, 3s3d–3s4f, $3p^2$–3s4f and 3p3d–3p4f transitions are presented in table 5. The theoretical wavelengths are seen to agree very well with the NIST data [24] (difference is only 0.1%–0.3%). There is also good agreement of 3%–20% for the transition rates for the

Table 4. Wavelengths (λ in Å), and radiative rates (A_r in 10^8 s^{-1}) for $3l_13l_2$–$3l_33l_4$ transitions of Mg-like iron. Comparison of present results (Cowan and RMBPT codes) with the NIST recommended data [24].

Low level		Upper level		λ (Å)			A_r (10^8 s^{-1})		
Configuration	*LSJ*	Configuration	*LSJ*	COWAN	RMBPT	NIST	COWAN	RMBPT	NIST
3s3p	^{3}P$_2$	3p^2	^{3}P$_2$	303.67	304.95	305.00	123	124	130
3s3p	^{3}P$_1$	3p^2	^{3}P$_1$	306.75	307.80	307.78	50.1	47.3	49.1
3s3p	^{3}P$_2$	3p^2	^{3}P$_1$	320.09	321.84	321.76	73.7	68.6	71
3s3p	^{3}P$_1$	3p^2	^{3}P$_0$	316.27	317.65	317.62	183	171	177
3s3p	^{3}P$_1$	3p^2	^{3}P$_2$	291.64	292.32	292.36	41.7	43.7	45
3s3p	^{3}P$_0$	3p^2	^{3}P$_1$	301.57	302.37	302.45	70.8	66.8	69
3s3p	^{3}P$_2$	3p^2	^{1}D$_2$	323.45	327.07	327.03	27.0	18.0	20
3s3p	^{3}P$_1$	3p^2	^{1}D$_2$	309.84	312.58	312.55	14.8	10.1	11
3s3p	^{1}P$_1$	3p^2	^{1}D$_2$	455.55	481.25	481.52	18.9	14.4	16
3s3p	^{3}P$_2$	3s3d	^{3}D$_3$	233.61	234.18	233.86	224	211	220
3s3p	^{3}P$_1$	3s3d	^{3}D$_2$	227.40	227.47	227.21	182	172	180
3s3p	^{3}P$_0$	3s3d	^{3}D$_1$	225.16	225.01	224.76	140	132	138
3s3p	^{3}P$_2$	3s3d	^{3}D$_2$	234.65	235.05	234.76	55.7	52.0	55
3s3p	^{3}P$_1$	3s3d	^{3}D$_1$	228.04	228.01	227.70	100	94.2	98
3s3p	^{3}P$_2$	3s3d	^{3}D$_1$	235.33	235.62	235.27	6.11	5.68	6.2
3s3p	^{1}P$_1$	3s3d	^{1}D$_2$	243.83	244.27	243.79	419	397	420
3s3p	^{3}P$_2$	3s3d	^{1}D$_2$	200.09	197.11	196.74	0.108	0.154	0.16
3s3p	^{3}P$_1$	3s3d	^{1}D$_2$	194.80	191.75	191.41	3.65	3.17	3.5
3s3d	^{3}D$_3$	3p3d	^{3}F$_4$	368.76	372.64	372.78	59.3	54.4	60
3s3d	^{3}D$_2$	3p3d	^{3}F$_3$	381.77	386.97	387.00	42.9	39.4	41
3s3d	^{3}D$_1$	3p3d	^{3}F$_2$	394.30	400.68	400.65	33.2	29.9	32
3s3d	^{3}D$_3$	3p3d	^{3}F$_3$	384.56	389.37	389.48	9.98	8.68	10
3s3d	^{3}D$_2$	3p3d	^{3}F$_2$	396.22	402.34	402.16	9.18	7.94	9.1
3s3d	^{3}D$_3$	3p3d	^{3}F$_2$	399.22	404.93	404.94	0.130	0.123	0.11

3s^2–3s4p, 3s3d–3s4f, 3p^2–3s4f and 3p3d–3p4f transitions; however, there is a much larger discrepancy for the 3s3p ^{1}P$_1$–3s4d ^{1}D$_2$ and 3p3d ^{3}F$_3$–3p4f ^{3}G$_4$ transitions.

Data for transitions between the $3ln_1l_1$ and $3l'n_2l_2$ states as well as between the $3ln_1l_1$ and $4l'n_2l_2$ states are illustrated in table 6. It should be noted that one does not need all 172 962 transitions to calculate the DR rate coefficients to excited states but rather only the transitions from the excited states (states under the first threshold 3s) to the autoionizing states (states above the first threshold 3s). The 3dnl states become autoionizing for $n \geqslant 7$, the 3pnl states for $n \geqslant 10$, and the 3snl states do not autoionize for any value of n. Thus, we obtain 56 875 transitions from the excited even-parity states to the $3lnl'$ autoionizing odd-parity states and 63 108 transitions from the excited odd-parity states to the $3lnl'$ autoionizing even-parity states. In table 6 the transitions with the largest intensity factor Q_d are presented as an example; these transitions will be discussed in the next section.

In the fifth column (heading A_a) of table 6, the autoionization rates relative to the first threshold, 3s, are given. The next column in table 6 shows autoionization rates as a sum of A_a (heading $\sum A_a$) calculated relative to the $3l$ thresholds with $l = 0, 1, 2$. The column with the heading E_S in table 6 lists excitation energies E_S relative to the first threshold 3s in eV. The E_S energy for the second and third thresholds is 36 eV and 84 eV, respectively. Of course, $\sum A_a$ is equal to A_a for $0 \leqslant E_S \leqslant 36$ eV.

Table 5. Wavelengths (λ in Å), and radiative rates (A_r in 10^8 s^{-1}) for $3l_13l_2$–$3l_34l_4$ transitions of Mg-like iron. Comparison of present results (Cowan code) with the NIST recommended data [24].

Low level		Upper level		λ (Å)		A_r (10^8 s^{-1})	
Configuration	*LSJ*	Configuration	*LSJ*	COWAN	NIST	COWAN	NIST
$3s^2$	$^1S_0$	3s4p	$^1P_1$	52.96	52.91	2538	2940
3s3p	$^1P_1$	3s4d	$^1D_2$	59.15	59.40	2468	3400
3s3p	$^3P_2$	3s4s	$^3S_1$	66.30	66.24	1917	1600
3s3p	$^3P_1$	3s4s	$^3S_1$	65.71	65.61	1175	980
3s3p	$^3P_0$	3s4s	$^3S_1$	65.47	65.37	399	320
3s3p	$^1P_1$	3s4s	$^1S_0$	69.46	69.7	2274	1900
3s3d	$^3D_3$	3s4f	$^3F_4$	70.24	70.05	8743	8800
3s3d	$^3D_2$	3s4f	$^3F_3$	70.16	69.99	7793	7900
3s3d	$^3D_1$	3s4f	$^3F_2$	70.11	69.94	7378	7400
3s3d	$^1D_2$	3s4f	$^1F_3$	73.24	73.47	6369	6200
$3p^2$	$^1D_2$	3s4f	$^1F_3$	64.27	63.96	1643	1600
3p3d	$^3F_3$	3p4f	$^3G_4$	69.30	68.86	7083	9200
3p3d	$^3D_3$	3p4f	$^3D_3$	70.60	70.59	1923	1700
3p3d	$^3P_0$	3p4f	$^3D_1$	70.30	70.22	4317	4130
3p3d	$^1F_3$	3p4f	$^1G_4$	73.01	73.20	7226	8800

3. Dielectronic satellite spectra

The DR process to the bound states of the Mg-like ion occurs as an electron capture by the Na-like ion to the autoionizing states of the Mg-like ion followed by the radiative decay to the singly-excited bound states:

$$\begin{aligned} \mathrm{Fe}^{15+}(3\mathrm{s}) + e \rightarrow \mathrm{Fe}^{14+*}(3\mathrm{p}n_1l_1 + 3\mathrm{d}n_2l_2 + 4ln_3l_3) \rightarrow \mathrm{Fe}^{14+*}(3\mathrm{s}nl_1' + 3\mathrm{p}nl_2' + 3\mathrm{d}nl_3') + h\nu \\ \downarrow \\ \mathrm{Fe}^{15+}(3\mathrm{s}, 3\mathrm{p}, 3\mathrm{d}) + e. \end{aligned} \tag{1}$$

The ground state of Fe^{15+}, 3s, is the initial state. The $3pn_1l_1$ ($n_1 \geqslant 10$), $3dn_2l_2$ ($n_2 \geqslant 7$) and $4ln_3l_3$ ($n_3 \geqslant 4$) levels are taken into account as autoionizing intermediate states.

During the DR process, the dielectronic satellite lines are emitted when the electron jumps from doubly-excited autoionization states to singly-excited bound states. Radiative transitions from the 3p*nl* states to 3s*nl* states and those from the 4p*nl* states to 3s*nl* states give rise to satellite lines of the 3p–3s and 4p–3s lines of the Na-like iron. There also exist DR satellite transitions from autoionizing states $3dnl$ to $3dn'l'$ and $3pnl$ to $3pn'l'$ with the change of the principal quantum number n. They appear at a shorter wavelength region.

The effective emission rate coefficient of the dielectronic satellite line is

$$C_S^{\mathrm{eff}}(j,i) = 3.3 \times 10^{-24} \left(\frac{I_H}{kT_e}\right)^{3/2} \frac{Q_d(j,i)}{g_0} \exp\left(-\frac{E_S(i)}{kT_e}\right) \text{ photons cm}^3 \text{ s}^{-1}, \tag{2}$$

where

$$Q_d(j,i) = \frac{g(i)A_a(i,i_0)A_r(j,i)}{\sum_{i_0'} A_a(i,i_0') + \sum_k A_r(k,i)}, \tag{3}$$

and I_H is the ionization potential of hydrogen, j denotes the bound state, i is the autoionizing state, i_0 is the initial state (that is, the ground state 3s of the Na-like ion), and i_0' is the possible final state for autoionization, e.g., 3s, 3p and 3d. The statistical weight of the initial

Table 6. Autoionization rates (A_a in s^{-1}) and excitation energies (E_S in eV) for even-parity states. Wavelengths (λ in Å), weighted radiative rates (gA_r in s^{-1}), intensity factors (Q_d in s^{-1}) and effective emission rate coefficients ($C_S^{\rm eff}$ in $cm^3\ s^{-1}$) for transitions between the excited and the $3lnl'$, $4lnl'$ autoionization states of Mg-like iron.

Low level		Upper level		A_a	ΣA_a	E_S	ΣgA_r	gA_r	λ	Q_d	$C_S^{\rm eff}$
Conf.	*LSJ*	Conf.	*LSJ*	(s^{-1})	(s^{-1})	(eV)	(s^{-1})	(s^{-1})	(Å)	(s^{-1})	($cm^3\ s^{-1}$)
$3d^2$	$^1G_4$	3d7f	$^1H_5$	3.41 [12]	3.41 [12]	20.535	3.30 [12]	2.23 [12]	40.90	2.05 [12]	6.89 [−13]
$3d^2$	$^3F_2$	3d7f	$^3G_3$	8.59 [12]	8.59 [12]	19.743	1.70 [12]	6.90 [11]	40.43	6.71 [11]	2.44 [−13]
$3d^2$	$^3F_3$	3d7f	$^3G_4$	4.37 [11]	4.37 [11]	20.006	2.12 [12]	9.89 [11]	40.43	6.43 [11]	2.28 [−13]
$3d^2$	$^3P_2$	3d7f	$^1F_3$	2.86 [13]	2.86 [13]	20.247	1.59 [12]	5.61 [11]	40.93	5.56 [11]	1.92 [−13]
$3d^2$	$^3P_2$	3d7f	$^3P_2$	1.98 [12]	1.98 [12]	20.210	9.79 [11]	4.40 [11]	40.94	4.00 [11]	1.39 [−13]
3d4d	$^3G_5$	3d7f	$^3H_6$	2.97 [11]	2.97 [11]	19.820	1.22 [12]	5.32 [11]	88.09	4.04 [11]	1.46 [−13]
3p3d	$^3F_4$	3d7d	$^3G_5$	3.54 [12]	3.54 [12]	18.425	1.44 [12]	7.56 [11]	34.69	7.29 [11]	3.02 [−13]
3p3d	$^1F_3$	3d7d	$^1G_4$	1.94 [13]	1.94 [13]	18.788	1.36 [12]	7.12 [11]	35.94	7.07 [11]	2.83 [−13]
3d4f	$^3H_6$	3d7g	$^3I_7$	3.17 [12]	3.17 [12]	20.384	1.55 [12]	5.59 [11]	92.66	5.42 [11]	1.85 [−13]
3d6h	$^3K_6$	3d7i	$^3L_7$	1.25 [12]	1.25 [12]	20.123	8.37 [11]	5.32 [11]	547.92	5.09 [11]	1.78 [−13]
3d6h	$^3K_7$	3d7i	$^3L_8$	1.26 [12]	1.26 [12]	20.126	9.48 [11]	6.04 [11]	548.18	5.78 [11]	2.02 [−13]
3p3d	$^3F_4$	3d8d	$^3G_5$	2.12 [12]	2.12 [12]	33.778	1.07 [12]	5.07 [11]	33.27	4.85 [11]	4.33 [−14]
3d4s	$^1D_2$	4s4f	$^1F_3$	9.06 [13]	9.06 [13]	30.199	7.83 [12]	4.59 [12]	68.32	4.53 [12]	5.79 [−13]
3d4s	$^3D_1$	4s4f	$^3F_2$	2.11 [13]	2.11 [13]	29.668	5.59 [12]	2.74 [12]	68.07	2.60 [12]	3.51 [−13]
3d4s	$^3D_2$	4s4f	$^3F_3$	2.13 [13]	2.13 [13]	29.761	7.93 [12]	4.06 [12]	68.08	3.85 [12]	5.14 [−13]
3d4s	$^3D_3$	4s4f	$^3F_4$	2.12 [13]	2.12 [13]	29.871	1.04 [13]	6.45 [12]	68.14	6.12 [12]	8.07 [−13]
3d4d	$^1D_2$	4d4f	$^1F_3$	4.03 [13]	5.42 [13]	65.350	9.22 [12]	3.77 [12]	67.83	2.74 [12]	1.04 [−14]
3d4d	$^1G_4$	4d4f	$^1H_5$	6.12 [13]	1.08 [14]	66.844	1.49 [13]	1.12 [13]	67.59	6.24 [12]	2.04 [−14]
3p4s	$^3P_2$	4s4d	$^3D_3$	4.93 [13]	4.93 [13]	21.290	4.77 [12]	2.69 [12]	55.95	2.65 [12]	8.25 [−13]
3d4p	$^3F_4$	4p4f	$^3G_5$	2.91 [12]	3.61 [12]	44.840	1.29 [13]	9.99 [12]	67.89	6.09 [12]	1.80 [−13]
3d4f	$^1G_4$	4f2	$^1G_4$	7.28 [13]	1.53 [14]	71.940	1.64 [13]	4.16 [12]	66.79	1.96 [12]	3.85 [−15]
3d4f	$^1F_3$	4f2	$^1G_4$	7.28 [13]	1.53 [14]	71.940	1.64 [13]	9.38 [12]	68.44	4.42 [12]	8.68 [−15]
3d4f	$^1D_2$	4f2	$^1D_2$	1.02 [13]	2.12 [13]	73.804	9.18 [12]	5.25 [12]	66.84	2.32 [12]	3.78 [−15]
3d6f	$^3H_6$	4f6f	$^3I_7$	3.53 [12]	2.26 [13]	182.873	1.58 [13]	1.20 [13]	66.64	1.79 [12]	5.34 [−20]

state i_0 is $g_0 = 2$, $g(i)$ is the statistical weight of the doubly-excited state, $A_a(i, i_0)$ is the autoionization rate from i to i_0, $A_r(j, i)$ is the radiative transition probability from i to j, $E_S(i)$ is the excitation energy of the autoionizing state i relative to the first threshold, 3s, and T_e is the electron temperature. A Maxwellian distribution is assumed for electron velocities. For some cases, $A_a \gg A_r$ and then Q_d is roughly estimated as $Q_d(j, i) \approx g(i)A_r(j, i)$.

As already mentioned above, autoionization rates $A_a(i, 3s)$, sum of autoionization rates $\sum A_a(i, i_0') = A_a(i, 3s) + A_a(i, 3p) + A_a(i, 3d)$ and excitation energies E_S for even- and odd-parity states are presented in columns 5, 6 and 7 of table 6. Weighted radiative rates $g_i A_r(j, i)$, sums of weighted radiative rates $\sum_k g_i A_r(k, i)$ and wavelengths λ for dipole-allowed transitions are given in columns 9, 8 and 10 of table 6, respectively. The last two columns list relative intensity factors $Q_d(j, i)$ and effective emission rate coefficients $C_S^{\rm eff}(j, i)$ defined by equation (2). The $C_S^{\rm eff}(j, i)$ values are given for $T_e = 10$ eV. The number of transitions listed in table 6 is limited by the largest values of relative intensity factors $Q_d(j, i)$, namely, $Q_d(j, i) > 4.0 \times 10^{11}\ s^{-1}$ for the $3l_1n_2l_2$–$3l_3n_4l_4$ transitions and $Q_d(j, i) > 1.8\times 10^{12}\ s^{-1}$ for the $3l_1n_2l_2$–$4l_3n_4l_4$ transitions. This leaves only 24 lines in table 6 out of total of more than 200 000 transitions. The largest value of $Q_d(j, i)$ gives the

Table 7. Total DR rate coefficients (in cm^3 s^{-1}) $\alpha_d^{\rm tot} = \alpha_d^{3a} + \alpha_d^{3b} + \alpha_d^{33} + \alpha_d^{4a} + \alpha_d^{4b}$. The contributions of α_d^{3a} and α_d^{3b} are the sums from the $3l_1n_1l_1$–$3l'nl$ transitions with $n = 10$–12 and $n = 13$–1000, respectively. The α_d^{33} is the contribution from the high states 3snl–3pnl transitions with $n = 13$–1000. The contributions of α_d^{4a} and α_d^{4b} are the sums from the $3l_1n_1l_1$–$4l'nl$ transitions with $n = 4$–7 and $n = 8$–1000, respectively. The $3l_1n_1l_1$ excited states include the 3sn_1l_1 ($n_1 = 3$–12), 3pn_1l_1 ($n_1 = 3$–9) and 3dn_1l_1 ($n_1 = 3$–6) configurations.

T_e	α_d^{3a}	α_d^{3b}	α_d^{33}	α_d^{4a}	α_d^{4b}	$\alpha_d^{\rm total}$
0.100	6.00 [−11]	3.24 [−70]	7.22 [−71]	1.72 [−12]	0.00 [00]	6.18 [−11]
0.130	6.45 [−11]	1.55 [−56]	3.46 [−57]	6.45 [−12]	0.00 [00]	7.10 [−11]
0.169	6.32 [−11]	4.90 [−46]	1.09 [−46]	1.73 [−11]	0.00 [00]	8.06 [−11]
0.220	5.90 [−11]	5.72 [−38]	1.27 [−38]	3.58 [−11]	0.00 [00]	9.48 [−11]
0.286	5.45 [−11]	9.38 [−32]	2.07 [−32]	6.02 [−11]	0.00 [00]	1.15 [−10]
0.371	5.22 [−11]	6.11 [−27]	1.33 [−27]	8.59 [−11]	0.00 [00]	1.38 [−10]
0.483	5.43 [−11]	3.42 [−23]	7.40 [−24]	1.07 [−10]	0.00 [00]	1.62 [−10]
0.627	6.24 [−11]	2.81 [−20]	6.14 [−21]	1.20 [−10]	0.00 [00]	1.82 [−10]
0.816	7.56 [−11]	5.13 [−18]	1.14 [−18]	1.21 [−10]	0.00 [00]	1.97 [−10]
1.060	9.14 [−11]	2.88 [−16]	6.64 [−17]	1.13 [−10]	1.10 [−82]	2.05 [−10]
1.379	1.06 [−10]	6.47 [−15]	1.55 [−15]	9.92 [−11]	3.46 [−66]	2.06 [−10]
1.792	1.18 [−10]	7.13 [−14]	1.80 [−14]	8.27 [−11]	1.76 [−53]	2.01 [−10]
2.330	1.24 [−10]	4.53 [−13]	1.21 [−13]	6.64 [−11]	1.09 [−43]	1.91 [−10]
3.029	1.26 [−10]	1.87 [−12]	5.59 [−13]	5.21 [−11]	3.76 [−36]	1.81 [−10]
3.937	1.25 [−10]	5.53 [−12]	1.98 [−12]	4.06 [−11]	2.34 [−30]	1.73 [−10]
5.119	1.22 [−10]	1.25 [−11]	5.67 [−12]	3.24 [−11]	6.62 [−26]	1.72 [−10]
6.654	1.16 [−10]	2.27 [−11]	1.32 [−11]	2.71 [−11]	1.74 [−22]	1.79 [−10]
8.650	1.08 [−10]	3.41 [−11]	2.48 [−11]	2.42 [−11]	7.42 [−20]	1.91 [−10]
11.245	9.71 [−11]	4.38 [−11]	3.81 [−11]	2.27 [−11]	7.83 [−18]	2.02 [−10]
14.619	8.40 [−11]	4.95 [−11]	4.94 [−11]	2.17 [−11]	2.81 [−16]	2.05 [−10]
19.005	7.01 [−11]	5.02 [−11]	5.55 [−11]	2.07 [−11]	4.33 [−15]	1.96 [−10]
24.706	5.64 [−11]	4.67 [−11]	5.58 [−11]	1.94 [−11]	3.42 [−14]	1.78 [−10]
32.118	4.40 [−11]	4.06 [−11]	5.13 [−11]	1.80 [−11]	1.59 [−13]	1.54 [−10]
41.754	3.34 [−11]	3.34 [−11]	4.39 [−11]	1.66 [−11]	4.83 [−13]	1.28 [−10]
54.280	2.47 [−11]	2.64 [−11]	3.57 [−11]	1.51 [−11]	1.06 [−12]	1.03 [−10]
70.564	1.80 [−11]	2.01 [−11]	2.78 [−11]	1.35 [−11]	1.77 [−12]	8.11 [−11]
91.733	1.29 [−11]	1.49 [−11]	2.09 [−11]	1.17 [−11]	2.43 [−12]	6.28 [−11]
119.253	9.10 [−12]	1.08 [−11]	1.54 [−11]	9.79 [−12]	2.84 [−12]	4.79 [−11]
155.029	6.37 [−12]	7.73 [−12]	1.11 [−11]	7.93 [−12]	2.92 [−12]	3.60 [−11]
201.538	4.42 [−12]	5.45 [−12]	7.84 [−12]	6.22 [−12]	2.73 [−12]	2.67 [−11]
261.999	3.05 [−12]	3.81 [−12]	5.50 [−12]	4.73 [−12]	2.37 [−12]	1.95 [−11]
340.599	2.09 [−12]	2.64 [−12]	3.82 [−12]	3.52 [−12]	1.94 [−12]	1.40 [−11]
442.779	1.43 [−12]	1.82 [−12]	2.64 [−12]	2.56 [−12]	1.52 [−12]	9.97 [−12]
575.612	9.74 [−13]	1.24 [−12]	1.81 [−12]	1.83 [−12]	1.15 [−12]	7.02 [−12]
748.296	6.63 [−13]	8.50 [−13]	1.24 [−12]	1.30 [−12]	8.50 [−13]	4.90 [−12]
972.784	4.50 [−13]	5.79 [−13]	8.45 [−13]	9.06 [−13]	6.14 [−13]	3.39 [−12]
1264.620	3.05 [−13]	3.93 [−13]	5.74 [−13]	6.29 [−13]	4.37 [−13]	2.34 [−12]
1644.005	2.06 [−13]	2.67 [−13]	3.90 [−13]	4.33 [−13]	3.07 [−13]	1.60 [−12]

largest value of effective emission rate coefficients $C_S^{\rm eff}(j,i)$ when the ratio of E_S and kT_e is not very large.

Figures 1 and 2 show examples of dielectronic satellite spectra for $kT_e = 10$ eV for two wavelength ranges. In these figures, we include data for 3322 even–odd parity transitions and 3901 odd–even parity transitions. The effective emission rate coefficients $C_S^{\rm eff}(j,i)$ and Gaussian profiles with spectral resolution $R \equiv \lambda/\Delta\lambda = 500$–700 are used to synthesize these

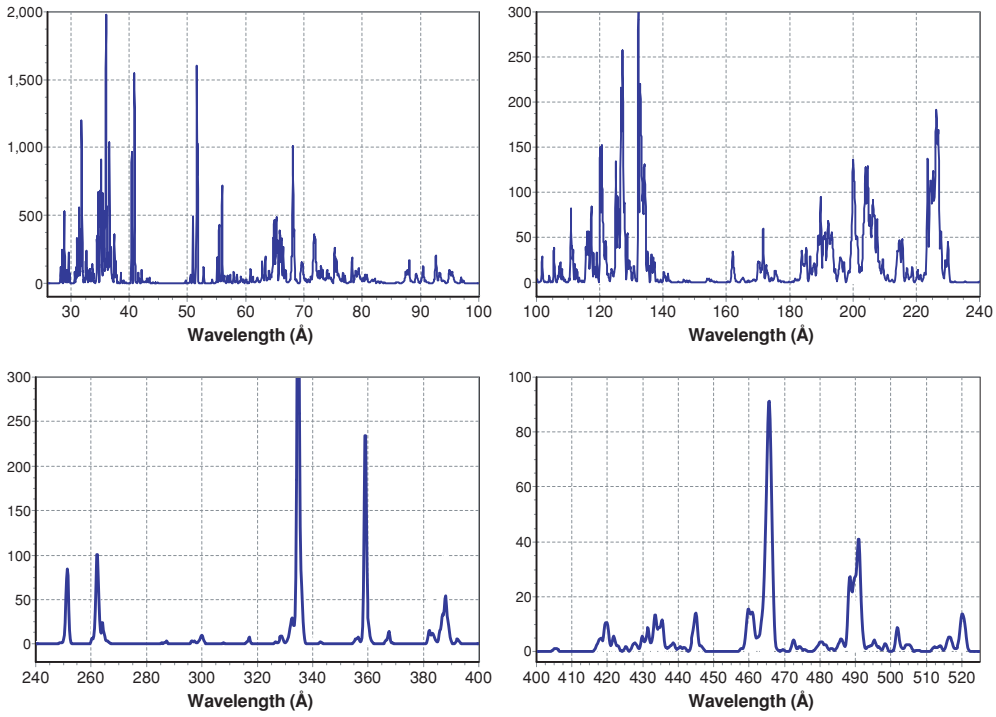

Figure 1. Convoluted Gaussian spectra of dielectronic satellite lines from Fe^{14+} ion at T_e = 10 eV for λ = 25–520 Å. Resolution $R = \lambda/\Delta\lambda = 500$ is assumed. The ordinate scale is in units of 10^{-15} cm^3 s^{-1}.

spectra. The limited set of transitions includes transitions with $C_S^{\rm eff}(j,i) > 10^{-15}$ cm^3 s^{-1}. The synthetic spectrum of dielectronic satellite lines from the Fe^{14+} ion at T_e = 10 eV is divided into eight parts: λ = 25 Å –100 Å , λ = 100 Å–240 Å , λ = 240 Å–400 Å and λ = 400 Å–520 Å (figure 1); λ = 520 Å–630 Å , λ = 660 Å–780 Å, λ = 840 Å–1040 Å and λ = 1400 Å–2000 Å (figure 2).

The strongest lines shown in figure 1 are due to the Rydberg transitions $3p^2$–3p10d, $3d^2$–3d7f, 3p4f–3p10g, 3p5d–3p10f, 3p5f–3p10g and 3p6f–3p10g (λ = 32 Å, 40 Å, 75 Å, 127 Å, 132 Å, 224 Å, respectively). The strongest lines in the region of 50 Å–65 Å are due to the 3p4s–4s4d, 3s4s–4s4p, 3p4p–4s4p and 3s4d–4s4p transitions. The last transition is the result of a strong mixing of configurations 3s4d and 3p4p. A large number of satellite lines to the 3s–3p transitions (3s10l–3p10l with l = 3–7) are responsible for the spectra shown in figure 1 in the region of λ = 330–335 Å. The strong contributions of the 3d6h–3d7i and 3d6g–3d7h transitions to the region of λ = 540–560 Å and the 3p8h–3p10i and 3p8i–3p10k transitions to the region of λ = 715–720 Å are shown in figure 2. There are contributions of the transitions 3p8h–3p11i and 3p8i–3p11k to the region of λ = 980–990 Å and 3p9i–3p10k transitions to the region of λ = 1710 Å.

4. Dielectronic recombination rate coefficients for excited states

The DR rate coefficients for excited states are obtained by summation of the effective emission rate coefficients $C_S^{\rm eff}(j,i)$ (equation (2)) for DR processes through all possible intermediate

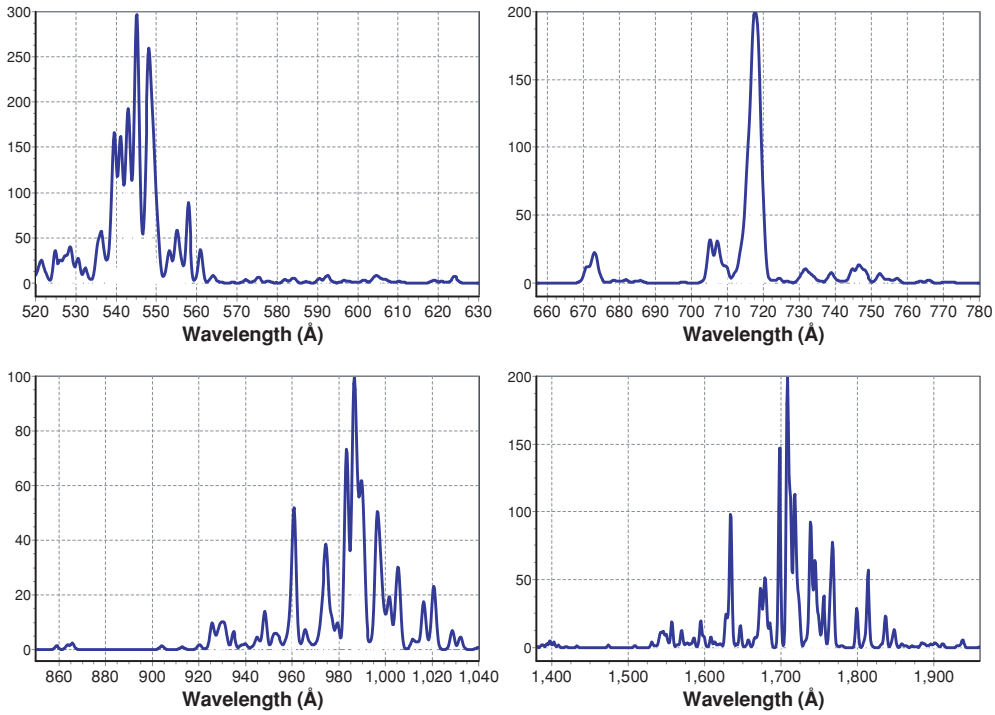

Figure 2. Convoluted Gaussian spectra of dielectronic satellite lines from Fe^{14+} ion at T_e = 10 eV for λ = 520–2000 Å. Resolution power $R = \lambda/\Delta\lambda = 700$ is assumed. The ordinate scale is in units of 10^{-15} cm^3 s^{-1}.

doubly-excited states:

$$\alpha_d(i_0, j) = \sum_i C_S^{\text{eff}}(j, i). \tag{4}$$

For the DR process described by equation (1), one has to calculate $\alpha_d(i_0, j)$ with i_0 = 3s and all possible excited states j of Fe^{14+} with energies below the first threshold, 3s (3686 000 cm^{-1}). Among the 3snl, (n = 3–12), 3pnl, (n = 3–9) and 3dnl, (n = 3–6) states, 444 states of odd parity and 419 states of even parity have energies lower than 3686 000 cm^{-1}.

The sum over i includes the autoionizing 3pnl states with $n \geqslant 10$, 3dnl states with $n \geqslant 7$ and 4lnl' states with $n \geqslant 4$. In figure 3, we illustrate the contributions to α_d(3s, j) for some of j's from the sum over i with n = 7–12 for autoionizing 3lnl' states and from the sum over i with n = 4–7 for autoionizing 4lnl' states. Those contributions are represented by curves 1 and 3, respectively. In figure 3, we show α_d(3s, j) with j = 3p3d ^{3}P$_1$, 3s4s ^{1}S$_0$, 3s4p ^{1}P$_1$ and 3s4f ^{3}F$_3$. One can see that the curves 1 are above the curves 3 for the 3p3d ^{3}P$_1$ level, while for 3s4s ^{1}S$_0$, the curves 1 are under the curves 3. For the 3s4p ^{1}P$_1$ and 3s4f ^{3}F$_3$ levels, the contributions of the 3lnl' autoionizing states are more important at low temperatures (1 eV to 5 eV) than the contributions of the 4lnl' autoionizing states, while at higher temperatures their relative contributions are opposite. It is clearly seen that the contribution of the 4lnl' in the sum over i in equation (4) is important for the calculation of α_d(3s, j) for different values of j.

In order to estimate contributions from the high-n autoionizing states to the DR rate coefficients for excited states (sum over i with $n > 12$ for autoionizing 3lnl' states and

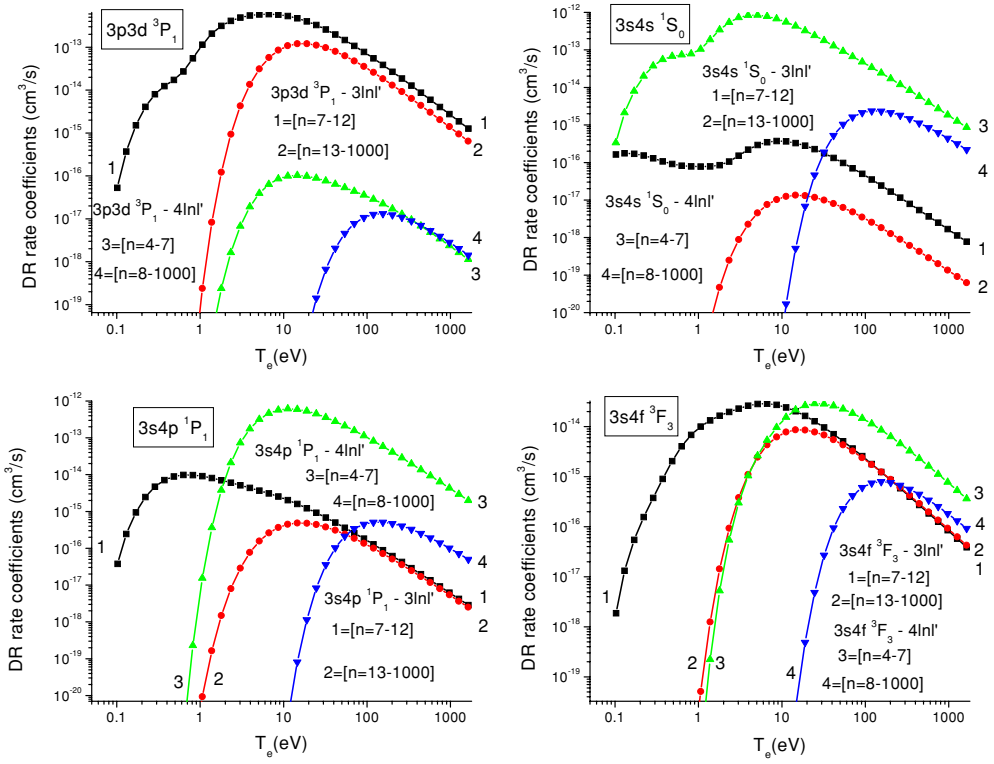

Figure 3. Contribution of the $3lnl'$ and $4lnl'$ states to the dielectronic recombination rate coefficient $\alpha_d(\gamma|3s)$ for the $3l3l'$ and $3l4l'$ states as a function of T_e in Mg-like Fe.

sum over i with $n > 7$ for autoionizing $4lnl'$ states), we use empirical scaling laws [12], which can only be implemented to include the one-electron 3s–*n*p, 3p–*n*s, 3p–*n*d, 3d–*n*p and 3d–*n*f dipole transitions. Additional contributions from the high-n states appear for the first low-lying configurations $3l3l'$ and $3l4l'$. For these configurations the [3s3p–3p*n*p], [3s3d–3d*n*p], [3p3d–3p*n*p, 3p*n*f, 3d*n*s, 3d*n*d], [3p^2–3p*n*s, 3p*n*d] and [3d^2–3d*n*p, 3d*n*f] transitions with $n > 12$ are to be included as well. Transitions with $n > 7$ are also taken into account for the $3l4l'$ configurations: [3s4s–4s*n*p], [3s4p–4p*n*p], [3s4f–4f*n*p], [3p4s–4s*n*s, 4s*n*d], [3p4p–4p*n*s, 4p*n*d], [3p4d–4d*n*s, 4d*n*d], [3p4f–4f*n*s, 4f*n*d], [3d4s–4s*n*p, 4s*n*f], [3d4p–4p*n*p, 4p*n*f], [3d4d–4d*n*p, 4d*n*f] and [3d4f–4f*n*p, 4f*n*f].

To estimate $Q_d(j,i)$ in equation (2) for autoionization states i with high principal quantum number n for the $3lnl'$ states and for the 3s–*n*p, 3p–*n*s, *n*d and 3d–*n*p, *n*f dipole transitions, we used our calculated data for $n = 11$ and the $1/n^3$ scaling law for rates A_a and A_r. For example, the formulae for the 3s3p–3p*n*p case are

$$A_a(3\mathrm{p}nl\,^{1,3}L_J) = \left(\frac{11}{n}\right)^3 A_a(3\mathrm{p}11l\,^{1,3}L_J), \tag{5}$$

$$A_r(3\mathrm{s}3\mathrm{p}\,^{1,3}\mathrm{P}_{J'}\text{–}3\mathrm{p}nl\,^{1,3}L_J) = \left(\frac{11}{n}\right)^3 A_r(3\mathrm{s}3\mathrm{p}\,^{1,3}\mathrm{P}_{J'}\text{–}3\mathrm{p}11l\,^{1,3}L_J) \times \left(\frac{\Delta E(3\mathrm{s}3\mathrm{p}\,^{1,3}\mathrm{P}_{J'}\text{–}3\mathrm{p}nl\,^{1,3}L_J)}{\Delta E(3\mathrm{s}3\mathrm{p}\,^{1,3}\mathrm{P}_{J'}\text{–}3\mathrm{p}11l\,^{1,3}L_J)}\right)^3. \tag{6}$$

In order to obtain the energies of the $3pnl\,^{1,3}L_J$ states as a function of nl, the following asymptotic formula was proposed in [28]:

$$E(3pnl) - E(3p) = -\frac{1}{2n^2}\left(Z - 11 + \frac{b(l)}{n}\right)^2, \tag{7}$$

where $b(s) = 2.873$, $b(p) = 1.761$, $b(d) = 0.721$, $b(f) = 0.137$ and $b(g) = 0.010$. The energy differences in equation (7) can be found using the following formula:

$$\Delta E(3s3p\,^{1,3}P_{J'}\text{–}3pnl\,^{1,3}L_J) = \Delta E(3s3p\,^{1,3}P_{J'}\text{–}3p11l\,^{1,3}L_J) - \frac{225}{2}\left(\frac{1}{n^2} - \frac{1}{11^2}\right) \times 219,474\,\mathrm{cm}^{-1}. \tag{8}$$

A similar formula was used for the excitation energies $E_S(i)$ in equation (4) when $i = 3pnl\,^{1,3}L_J$:

$$E_S(3pnl\,^{1,3}L_J) = E_S(3p11l\,^{1,3}L_J) - \frac{225}{2}\left(\frac{1}{n^2} - \frac{1}{11^2}\right) \times 219,474\,\mathrm{cm}^{-1}. \tag{9}$$

Using these scaling formulae for $A_a(3pnl\,^{1,3}L_J)$ and $A_r(3s3p\,^{1,3}P_{J'}\text{–}3pnl\,^{1,3}L_J)$, we calculated $Q_d(3s3p\,^{1,3}P_{J'}\text{–}3pnl\,^{1,3}L)$ as a function of n and then, using equation (9) for E_S, the sums over n for $\alpha_d(3s, 3s3p\,^{1,3}P_J)$ versus T_e.

To estimate $Q_d(j, i)$ in equation (2) for autoionizing states i with high principal quantum number n for the $3l4l'$ states (for example, for the 3s4s–4snp dipole transitions) we used the calculated data for $n = 7$ and the $1/n^3$ scaling law for A_a and A_r as was shown above in equations (5)–(9).

The results of the calculations are shown in figure 3. In order to test the scaling, the explicitly calculated data for $n = 12$ and the scaled data for $n = 12$ derived from the calculated data for $n = 11$ were compared. It was found that the difference is within 10% except for some cases when mixing of configurations is very important. In figures 3–5, the contribution of scaled data from $n = 12$ up to $n = 1000$ (curve 2) for the $3lnl'$ autoionizing states and from $n = 8$ up to $n = 1000$ (curve 4) for the $4lnl'$ autoionizing states are presented. The dependence of the present results on the upper limit of n was also investigated. We found that there is a small difference for low temperature (4% for $T_e = 10$ eV) with $n = 40$ as an upper limit, and the difference increases for high temperatures reaching 7% for $T_e = 30$ eV.

The high-n state contributions are very important for high temperatures. One can see from figure 3 that for $T_e > 10$ eV, the curves 2 describing contributions of the high $3lnl'$ states with $n = 13$–1000 are higher than the curves 1 describing contributions of the low $3lnl'$ states $n = 7$–12 (see the plot for the 3s4f $^3F_3$ level). The contribution of the high $4lnl'$ states becomes important for very high $T_e > 100$ eV. The curves 4 describing contributions of the high $4lnl'$ states with $n = 8$–1000 are in most cases below the curves 3 showing contributions of the low $4lnl'$ states with $n = 4$–7; however, the curves 4 are above curves 2 and 1 for 3s4s $^1S_0$, 3s4p $^1P_1$ and 3s4f $^3F_3$. The sum of the contributions presented by the curves 1, 2, 3 and 4 gives the DR rate coefficients for excited states.

The calculated values of $\alpha_d(3s, j)$ are presented in figure 4 (j corresponds to $3l3l'$), figure 5 ($3l4l'$—even-parity j's) and figure 6 ($3l4l'$—odd-parity j's). In these figures, $\alpha_d(3s, j)$ are shown for the six $3l3l'$ configurations and twelve $3l4l'$ configurations. The electron temperature for these plots varies from $T_e = 0.1$ eV to $T_e = 1600$ eV. As can be seen from figures 4–6, the DR rate coefficients can be divided into three different groups. There are curves without any maximum as, e.g., $\alpha_d(3s, j)$ for $j = 3p^2\,^1D_2\,^1S_0$, $^3P_0$, $^3P_1$ and 3s3d $^1D_2$ (figure 4). Then, there are curves with two maxima (at about 0.6–0.8 eV and 19.0 eV), e.g., $\alpha_d(3s, j)$ for $j = 3d4s\,^3D_J$ (figure 5) and 3p4s $^3P_0$, $^3P_1$ (figure 6). Most of the DR rate coefficients exhibit only one maximum around 0.8 eV to 2.3 eV or 19.0 eV.

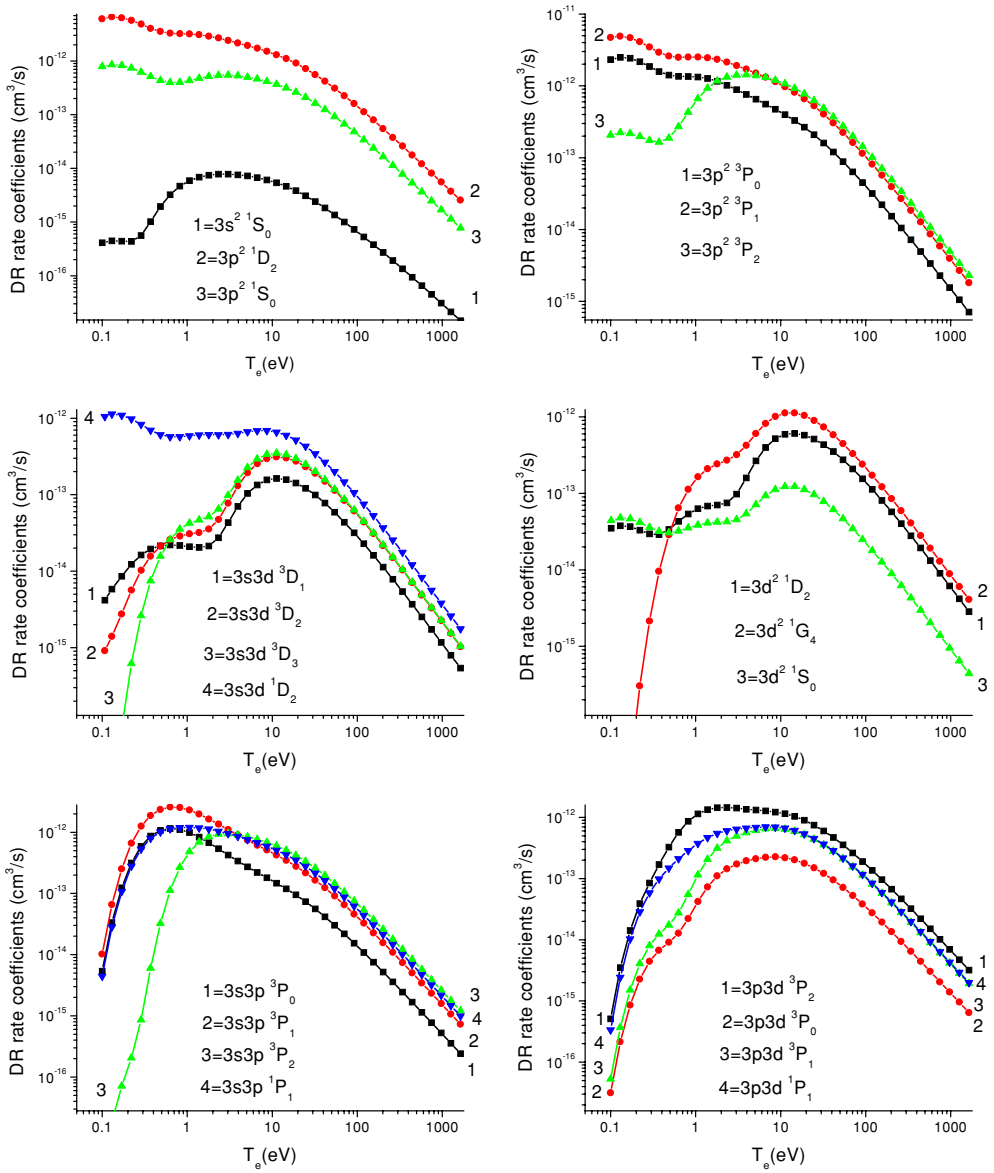

Figure 4. Dielectronic recombination rate coefficient $\alpha_d(\gamma|3s)$ for the $3l3l'$ states as a function of T_e in Mg-like Fe.

5. Total dielectronic recombination rate coefficients

The total DR rate coefficients are obtained by summation of the effective emission rate coefficients $C_S^{\rm eff}(j,i)$ (equation (2)) through all possible intermediate singly and doubly-excited states:

$$\alpha_d(i_0) = \sum_i \sum_j C_S^{\rm eff}(j,i). \tag{10}$$

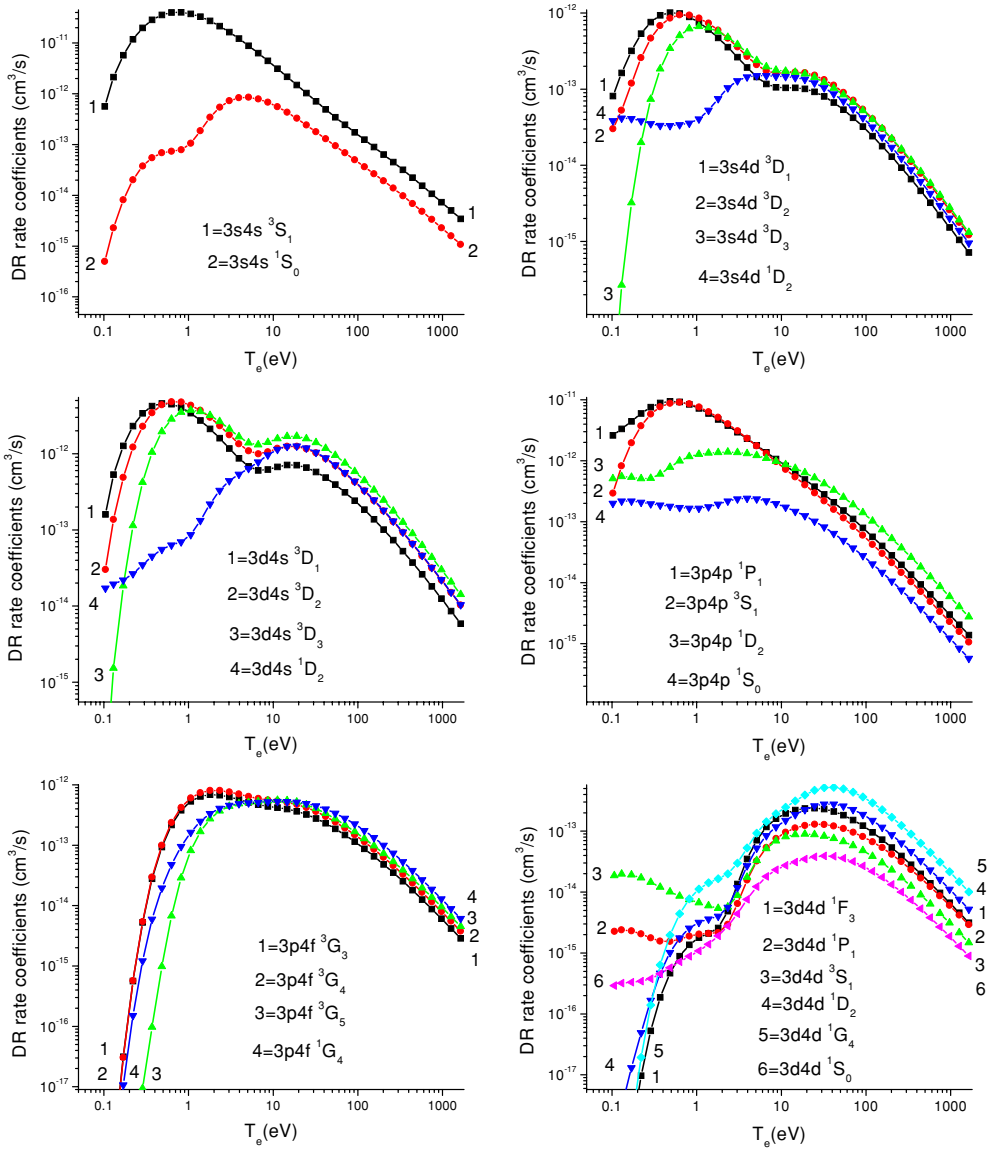

Figure 5. Dielectronic recombination rate coefficient $\alpha_d(\gamma|3s)$ for the $3l4l'$ even-parity states as a function of T_e in Mg-like Fe.

We have already discussed the contribution from doubly-excited states with high-n levels to the DR rate coefficients (sum over i in equation (4)). For the total DR rate coefficients one has to consider also the contribution from singly-excited states with high n, i.e., the 3snl states. For these states, the most important transitions are 3snl–3pnl [12, 14, 15, 18, 17].

To estimate $Q_d(j,i)$ in equation (3) for $j = 3snl$ and $i = 3pnl$ for $n > 12$, we used the calculated data for $n = 11$ and the $1/n^3$ scaling law for A_a (equation (5)) and E_S (equation (9)). The values of A_r for the 3snl–3pnl transitions are almost independent of n since this is a one-electron 3s–3p transition. One has to take into account the change of the energy difference

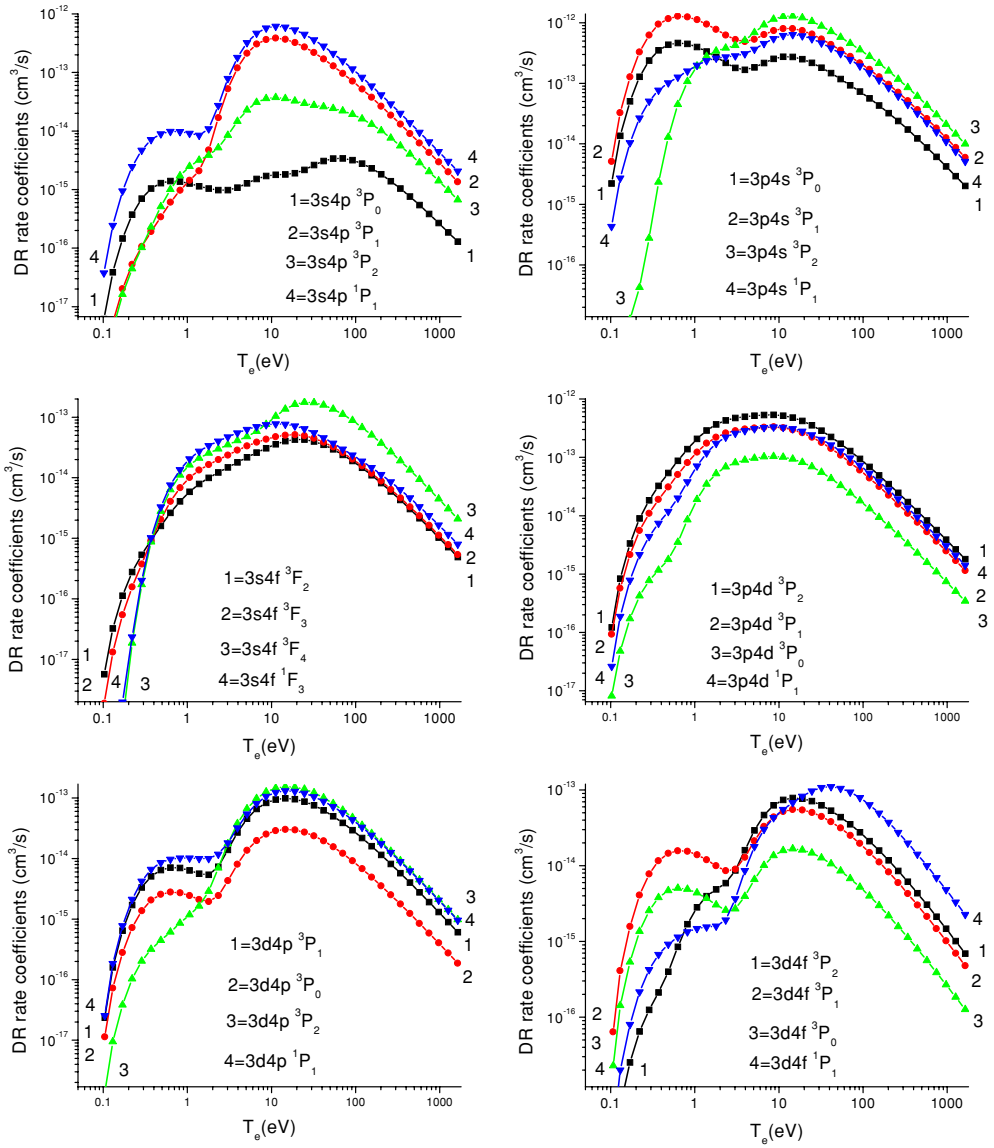

Figure 6. Dielectronic recombination rate coefficient $\alpha_d(\gamma|3s)$ for the $3l4l'$ odd-parity states as a function of T_e in Mg-like Fe.

following equation (7):

$$A_r(3snl\,^{1,3}L'_{J'}\text{–}3pnl\,^{1,3}L_J) = A_r(3s11l\,^{1,3}L'_{J'}\text{–}3p11l\,^{1,3}L_J) \times \left(\frac{\Delta E(3snl\,^{1,3}L'_{J'} - 3pnl\,^{1,3}L_J)}{\Delta E(3s11l\,^{1,3}L'_{J'} - 3p11l\,^{1,3}L_J)}\right)^3. \tag{11}$$

Using the asymptotic formula given by equation (8), we obtain in the first approximation:

$$\Delta E(3snl\,^{1,3}L'_{J'}\text{–}3pnl\,^{1,3}L_J) = \Delta E(3s11l\,^{1,3}L'_{J'}\text{–}3p11l\,^{1,3}L_J) \tag{12}$$

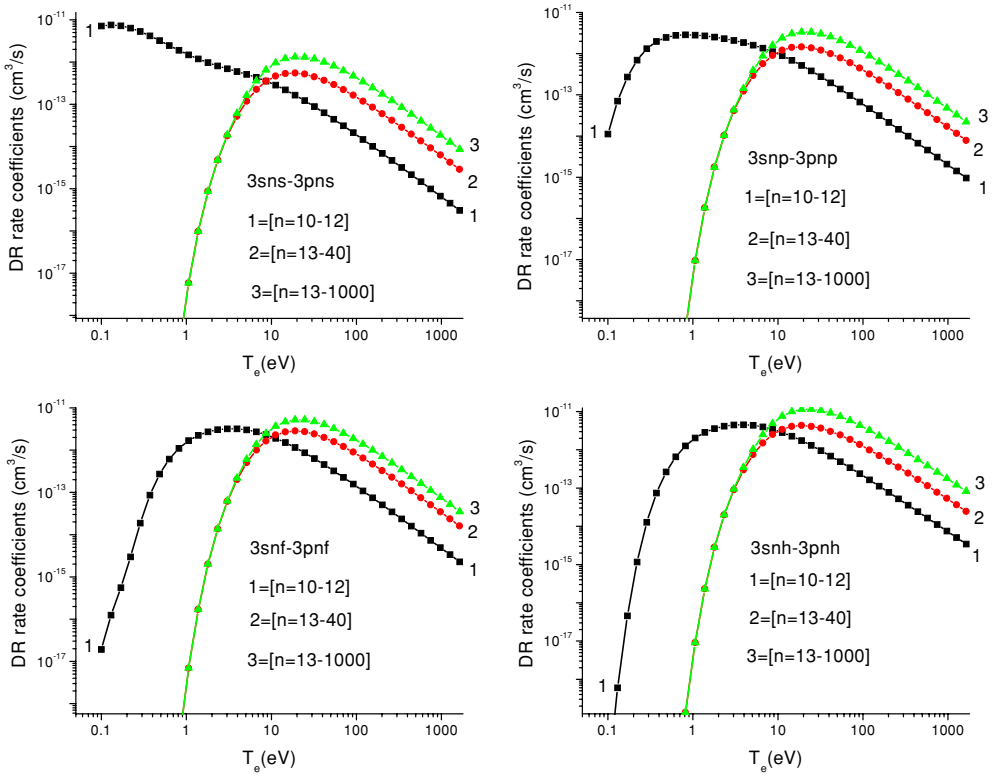

Figure 7. The 3snl–3pnl contribution of high states to the total DR rate coefficient $\alpha_d(3s, j)$ in sum over i and j in equation (10).

and finally [14]:

$$A_r(3snl\,^{1,3}L'_{J'}\text{–}3pnl\,^{1,3}L_J) = A_r(3s11l\,^{1,3}L'_{J'}\text{–}3p11l\,^{1,3}L_J). \tag{13}$$

Again, the calculated data for $n = 11$ and the $1/n^3$ scaling law for A_a were used for estimates of $Q_d(j, i)$ in equation (3) for autoionization states i with high n. For the 3snl–3pnl transitions, the scaling begins from $n = 12$. Using the scaling formulae for $A_r(3snl\,^{1,3}L'_{J'}\text{–}3pnl\,^{1,3}L_J)$ (equation (13)) and $A_a(3pnl\,^{1,3}L_J)$ (equation (5)), we calculated $Q_d(3snl\,^{1,3}L'_{J'}\text{–}3pnl\,^{1,3}L_J)$ and then, using equation (9) for E_S, we calculated $C_S^{\rm eff}(3snl\,^{1,3}L'_{J'}\text{–}3pnl\,^{1,3}L_J)$. The sums over LSJ and for $C_S^{\rm eff}(3snl\,^{1,3}L'_{J'}\text{–}3pnl\,^{1,3}L_J)$ give data for $C_S^{\rm eff}(3snl\text{–}3pnl)$ as a function of nl and T_e.

The results of calculations for $C_S^{\rm eff}(3snl\text{–}3pnl)$ are illustrated in figure 7 for the 3sns–3pns, 3snp–3pnp, 3snf–3pnf and 3snh–3pnh transitions. In figure 7, we demonstrate the contribution of scaled data for $n = 13$ to $n = 40$ (curves 2), and for $n = 13$ to $n = 1000$ (curves 3). As one can see from these plots, the difference between the results calculated with $n \leqslant 40$ and $n \leqslant 1000$ increases with increasing temperature (20–30% for $T_e = 5$ eV, 50–70% for $T_e = 19$ eV). It is worth noting that the convergence for the 3snl–3pnl transitions is slower than for the $3l_13l_2$–$3lnl'$ and $3l_14l_2$–$4lnl'$ transitions considered in the previous section. The results for the summed calculated data for $C_S^{\rm eff}(3lnl\text{–}3pnl)$ from $n = 10$–12 are also presented in figure 7 (curve 1). As can be seen from this plot, the curves 1 are above the curves 2 and 3

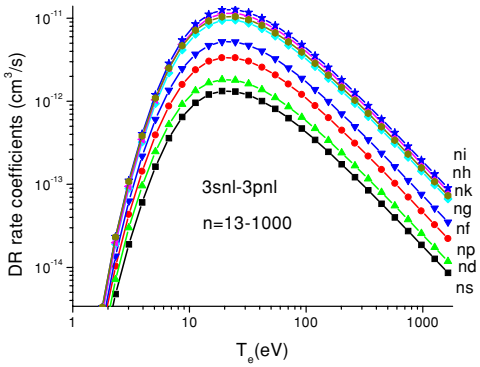

Figure 8. The 3snl–3pnl contribution of high states to the total DR rate coefficient α_d(3s, j) as a function of T_e for $l = 0$–7.

describing the scaled data only for low electron temperature. For $T_e > 10$ eV, the curves 1 are under the curves 2 ($n = 13$–40) and the curves 3 describing contribution from the scaled data for $n = 13$ to $n = 1000$. We already mentioned that the importance of the contributions from highly-excited states for the DR rate coefficients was emphasized by Hahn [29] and confirmed by the results of [12, 14, 15, 17, 18].

The final result of our 3snl–3pnl scaling is shown in figure 8. In this figure, $\sum_{n=13}^{n=1000} C_S^{\rm eff}$(3s$nl$–3p$nl$) is presented as a function of T_e for different values of l. As can be seen from figure 8, the value of this parameter increases with increasing l up to $l = 6$ (curve 'ni'), while for $l = 7$ (curve 'nk') it becomes smaller.

The total DR rate coefficients ($\alpha_d^{\rm tot}$ in cm^3 s^{-1}) are calculated as a sum of five terms: α_d^{3a}, α_d^{3b}, α_d^{33}, α_d^{4a} and α_d^{4b}. The contributions of α_d^{3a} and α_d^{3b} are the sums over the $3l_1n_2l_2$–$3l'nl$ transitions with $n = 10$–12 and $n = 13$–1000, respectively. The parameter α_d^{33} is the contribution from the high states 3snl–3pnl transitions with $n = 13$–1000. The contributions of α_d^{4a} and α_d^{4b} are the sums over the $3l_1n_1l_1$–$4l'nl$ transitions with $n = 4$–7 and $n = 8$–1000, respectively. The $3l_1n_1l_1$ excited states include the $3sn_1l_1$ states with $n_1 = 3$–12 and $l_1 = 0$–7, $3pn_1l_1$ states with $n_1 = 3$–9 and $l_1 = 0$–7, and $3dn_1l_1$ states with $n_1 = 3$–6 and $0 \leqslant l_1 \leqslant n_1 - 1$.

The results for α_d^{3a}, α_d^{3b}, α_d^{33}, α_d^{4a} and α_d^{4b} are shown in figure 9. The electron temperature for these plots varies from 0.1 eV–1600 eV. It is clearly seen that low excited states are responsible for the total DR rate coefficient at low T_e, and contribution from the high-n excited states becomes more important with increasing temperature. The curves describing the contribution of the $3l_1n_2l_2$–$3l'nl$, 3snl–3pnl and $3l_1n_1l_1$–$4l'nl$ transitions have maximums near 19 eV, 24 eV and 155 eV, respectively.

The tabulated data α_d^{3a}, α_d^{3b}, α_d^{33}, α_d^{4a}, α_d^{4b}, and their sum $\alpha_d^{\rm tot}$ are given in table 7 as a function of electron temperature T_e in the interval 0.1 eV–1624 eV on a logarithmic grid $T_e = (0.1 \times 1.3^{N-1})$ eV with $N = 1$–38 .

The sum of the scaled data $\left(\alpha_d^{3b} + \alpha_d^{33} + \alpha_d^{4b}\right)$ and sum of the calculated results $\left(\alpha_d^{3a} + \alpha_d^{4b}\right)$ are shown in figure 10. The contribution from the low excited states is responsible for the total DR rate coefficient at low T_e, and contribution from the high-n excited states becomes more important with increasing temperature. The curve describing the contribution of these states has a maximum near 19 eV. The resulting curve for the total DR rate coefficient $\alpha_d^{\rm tot}$ has two maxima for T_e near 1.4 eV and 14.6 eV. Our results are compared in figure 10 with the results of Gu [8]. As can be seen from this figure, the values of α_d(3s) from [8] agree well

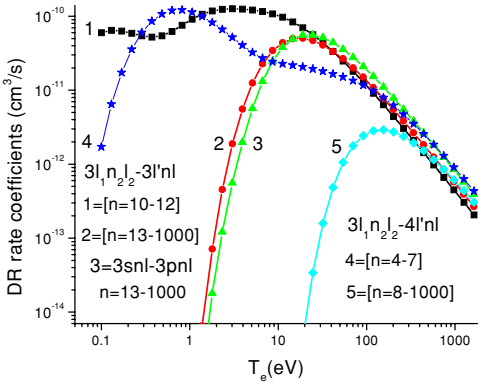

Figure 9. The contribution of the $3l_1n_1l_1$–$3l'nl$, $3snl$–$3pnl$ and $3l_1n_1l_1$–$4l'nl$ transition to the total DR rate coefficient $\alpha_d(3s,\ j)$ as a function of n and T_e in Mg-like iron. The $3l_1n_1l_1$ excited states include the $3sn_1l_1$ ($n_1 = 3$–12), $3pn_1l_1$ ($n_1 = 3$–9) and $3dn_1l_1$ ($n_1 = 3$–6) configurations.

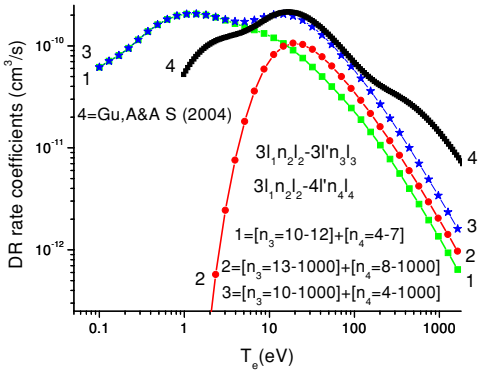

Figure 10. Total DR rate coefficient (α_d^{total}) as a function of T_e in Mg-like iron. For comparison the results of Gu [8] are presented as well.

with our data for 10 eV $< T_e <$ 100 eV. The disagreement for high T_e could be explained by the inner-shell excitation of a $2l$ electron with the maximum in the region of T_e equal to 200 eV [8]. The source of the disagreement for small T_e is not clear since the results for low T_e are given in [8] starting from $T_e = 1$ eV only.

6. Conclusion

In the present paper, we calculate a large set of atomic data related to dielectronic recombination of the astrophysically important Na-like ion of Fe into Mg-like Fe^{14+}.

Energy levels, wavelengths, weighted radiative transition probabilities and autoionization rates are calculated for the Mg-like iron ion using two theoretical methods, namely, the Hartree–Fock-relativistic method (Cowan code) and the relativistic many-body perturbation theory method for a limited number of states. The calculated atomic data are used to obtain the dielectronic satellite lines as well as the DR rate coefficients.

We take into account doubly-excited states $3pnl$ ($n \geqslant 10, l \leqslant 7$), $3dnl$ ($n \geqslant 7, l \leqslant n-1$) and $4l'nl$ ($n \geqslant 4, l \leqslant n-1$) as intermediate resonance states with n up to 1000 to calculate

the DR rate coefficients. Most of the state-selective DR rate coefficients show double peaks as a function of electron temperature. The transitions through intermediate states $3lnl$ and $4lnl$ make a peak in the DR rate coefficients at T_e about 0.6–0.8 eV and 19.0 eV. We also found that configuration mixing for [3sns + 3pnp + 3dnd] and [3snp + 3pns + 3pnd + 3dnp] states plays an important role for the DR rate coefficients of 3snl levels with $n \leqslant 7$ at low temperature.

We calculated the state-selective DR rate coefficients from the ground state of Na-like Fe ion to the bound states of Mg-like Fe ion in this paper. The total DR rate coefficient is in good agreement with the previous results by Gu [8] for medium temperatures.

The state selective rate coefficients can be used in collisional-radiative modelling for investigation of population kinetics and plasma diagnostics in recombining plasmas. We plan to calculate spectral line intensities of Mg-like Fe ions in a collisional-radiative model with the DR rate coefficients obtained in this paper to compare with measurements of laboratory plasmas.

Acknowledgments

This work was supported in part by the DOE-NNSA/NV Cooperative Agreement DE-FC52-01NV14050 (UIS and TEC), by the Office of Fusion Energy Sciences of the US Department of Energy (YuR), by the JSPS Grants-in-Aid for Scientific Research 15540479 (IM and TK) and by Matsuo Foundation (IM, DK, and TK). UIS would like to thank the members of the Atomic and Molecular Data Research Center, the National Institute for Fusion Science for their hospitality and financial support. UIS would like to thank Dr A Kramida for supervising the use of his version of the Cowan code. We are grateful to Dr M F Gu for sending tabulated data used in figure 10 of the present paper.

References

[1] May M J *et al* 2005 *Astrophys. J. Suppl.* **158** 230
[2] LaGattuta K J and Hahn Y 1984 *Phys. Rev.* A **30** 316
[3] Griffin D C and Pindzola 1987 *Phys. Rev.* A **36** 2821
[4] Gorczyca T W and Badnell N R 1990 *Phys. Rev.* A **54** 4113
[5] Linkemann J *et al* 1995 *Nucl. Instrum. Methods Phys. Res.* B **98** 154
[6] Kraemer S B, Ferland G L and Gabel J R 2004 *Astrophys. J.* **604** 556
[7] Netzer H 2004 *Astrophys. J.* **604** 551
[8] Gu M F 2004 *Astrophys. J. Suppl.* **153** 389
[9] Zhang H L, Sampson D H, Clark R E H and Mann J B 1989 *At. Data Nucl. Data Tables* **41** 1
[10] Chen M H 1989 *Phys. Rev.* A **40** 2365
[11] Nilsen J 1989 *At. Data Nucl. Data Tables* **41** 131
[12] Safronova U I and Kato T 1998 *J. Phys. B: At. Mol. Opt. Phys.* **31** 2501
[13] Safronova U I and Kato T 1996 *Phys. Scr.* **53** 461
[14] Kato T, Safronova U I and Ohira M 1997 *Phys. Scr.* **55** 185
[15] Safronova U I, Kato T and Ohira M 1997 *J. Quant. Spectrosc. Radiat. Transfer* **58** 193
[16] Murakami I, Safronova U I, Vasilyev A A and Kato T 2005 *At. Data Nucl. Data Tables* **90** 1
[17] Murakami I, Safronova U I and Kato T 2002 *Can. J. Phys.* **80** 1525
[18] Murakami I, Safronova U I and Kato T 1999 *J. Phys. B: At. Mol. Opt. Phys.* **32** 5351
[19] Mohr P J and Taylor B N The 2002 CODATA recommended values of the fundamental physical constants, Web Version 4.0, available at http://physics.nist.gov/constants
[20] Cowan R D 1981 *The Theory of Atomic Structure and Spectra* (Berkeley: University of California Press)
[21] URL http://das101.isan.troitsk.ru/cowan.htm
[22] Safronova M S, Johnson W R and Safronova U I 1996 *Phys. Rev.* A **53** 4036
[23] Safronova U I, Johnson W R and Berry H G 2000 *Phys. Rev.* A **61** 52503

[24] Ralchenko Yu, Jou F-C, Kelleher D E, Kramida A E, Musgrove A, Reader J, Wiese W L and Olsen K 2005 NIST Atomic Spectra Database (version 3.0.2) (Gaithersburg, MD: National Institute of Standards and Technology) Available at http://physics.nist.gov/asd3 (2006, January 4)
[25] Bhatia A K, Mason H E and Blancard C 1997 *At. Data Nucl. Data Tables* **66** 83
[26] Deb N C and Msezane A Z 1998 *J. Phys. B: At. Mol. Opt. Phys.* **31** L281
[27] Deb N C, Aggarwal K M and Msezane A Z 1999 *Astrophys. J. Suppl.* **121** 265
[28] Safronova U I, Tolstikhina I Y, Bruch R, Tanaka T, Hao F and Schneider D 1993 *Phys. Scr.* **47** 364
[29] Hahn Y 1985 *Adv. At. Mol. Phys.* **21** 123